

Surface Plasmon Resonance Analysis of Antibiotics Using Imprinted Boronic Acid-Functionalized Au Nanoparticle Composites

Marco Frasconi, Ran Tel-Vered, Michael Riskin, and Itamar Willner*

Institute of Chemistry, Center for Nanoscience and Nanotechnology, The Hebrew University of Jerusalem, Jerusalem 91904, Israel

Au nanoparticles (NPs) are functionalized with thioaniline electropolymerizable groups and (mercaptophenyl)boronic acid. The antibiotic substrates neomycin (NE), kanamycin (KA), and streptomycin (ST) include vicinal diol functionalities and, thus, bind to the boronic acid ligands. The electropolymerization of the functionalized Au NPs in the presence of NE, KA, or ST onto Au surfaces yields bisaniline-cross-linked Au NP composites that, after removal of the ligated antibiotics, provide molecularly imprinted matrixes which reveal high sensitivities toward the sensing of the imprinted antibiotic analytes (detection limits for analyzing NE, KA, and ST correspond to 2.00 ± 0.21 pM, 1.00 ± 0.10 pM, and 200 ± 30 fM, respectively). The antibiotics are sensed by surface plasmon resonance (SPR) spectroscopy, where the coupling between the localized plasmon of the NPs and the surface plasmon wave associated with the Au surface is implemented to amplify the SPR responses. The imprinted Au NP composites are, then, used to analyze the antibiotics in milk samples.

Residual quantities of antibiotics in milk or meat products were identified as health hazards, and maximum residue limits (MRLs) for these antibiotics were defined by the food administration authorities.¹ Scheme 1 outlines some commonly used antibiotics and their respective MRL values. Different sensing platforms for the analysis of different antibiotics were developed. For example, a competitive impedimetric immunosensor assay for analyzing ciprofloxacin, an antibiotic belonging to synthetic fluoroquinolones, was developed using polypyrrole-modified electrodes functionalized with the antibody–antibiotic analogue complexes.² An imaging surface plasmon resonance-based immunosensor was implemented for the simultaneous detection of several antibiotics in milk.³ Also, different sensing platforms that use antigen–antibody

complexes were used to detect a variety of antibiotics.⁴ Recently, wavelength-interrogated optical biosensors based on the formation of antibody–antibiotic antigen complexes were developed and used for the multiplexed screening of antibiotics in milk.⁵ Similarly, a lab-on-a-chip antibody-based sensing platform for the multiplexed analysis of antibiotics was described.⁶ Albeit the progress in the development of bioanalytical sensing platforms, the antibody-based sensors require long analysis times, and they do not reach the satisfactory sensitivities.

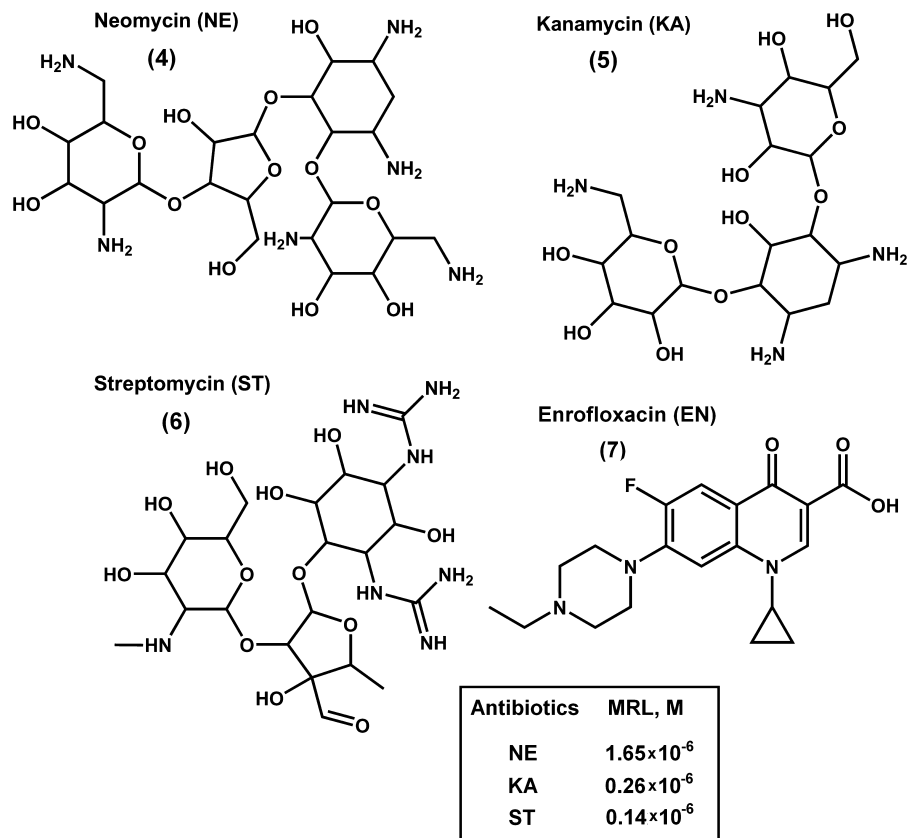
Surface plasmon resonance (SPR) is a versatile method to follow refractive index changes that occur on thin metal films (e.g., Au or Ag) as a result of recognition events or chemical transformations.⁷ SPR spectroscopy has been widely used to develop optical sensors and biosensors.⁸ For example, antigen–antibody complexes formed on the metal supports,⁹ enzyme-mediated transformations,¹⁰ or redox reactions proceeding on metallic films¹¹ were probed by SPR spectroscopy. The method is, however, limited to high-molecular-weight substrates, such as proteins, or low-molecular-weight substrates that undergo color changes upon chemical transformations that yield refractive index changes observable by SPR. This limitation can be resolved, however, by the conjugation of labels that amplify the refractive index changes that occur upon low coverage of the surface with

* To whom correspondence should be addressed. E-mail: willnea@vms.huji.ac.il. Phone: +972-2-6585272. Fax: +972-2-6527715.

- (1) (a) *Off. J. Eur. Union, L. Legis. (Engl. Ed.)* **1990**, L224, Paper No. EEC No. 2377/90. (b) Neubert, H.-J. *Anal. Chem.* **2006**, *78*, 7908.
- (2) (a) Ionescu, R. E.; Jaffrezic-Renault, N.; Bouffier, L.; Gondran, C.; Cosnier, S.; Pinacho, D. G.; Marco, M.-P.; Sánchez-Baeza, F. J.; Healy, T.; Martelet, C. *Biosens. Bioelectron.* **2007**, *23*, 549–555. (b) Giroud, F.; Gorgy, K.; Gondran, C.; Cosnier, S.; Pinacho, D. G.; Marco, M.-P.; Sánchez-Baeza, F. J. *Anal. Chem.* **2009**, *81*, 8405–8409.
- (3) Raz, S. R.; Bremer, M. G. E. G.; Haasnoot, W.; Norde, W. *Anal. Chem.* **2009**, *81*, 7743–7749.

- (4) (a) Kloth, K.; Rye-Johnsen, M.; Didier, A.; Dietrich, R.; Märklbauer, E.; Niessner, R.; Seidel, M. *Analyst* **2009**, *134*, 1433–1439. (b) Ferguson, J. P.; Baxter, G. A.; McEvoy, J. D. G.; Stead, S.; Rawlings, E.; Sharman, M. *Analyst* **2002**, *127*, 951–956. (c) Knecht, B. G.; Strasser, A.; Dietrich, R.; Märklbauer, E.; Niessner, R.; Weller, M. G. *Anal. Chem.* **2004**, *76*, 646–654. (d) Strasser, A.; Dietrich, R.; Usleber, E.; Märklbauer, E. *Anal. Chim. Acta* **2003**, *495*, 11–19.
- (5) (a) Adrian, J.; Pasche, S.; Pinacho, D. G.; Font, H.; Diserens, J.-M.; Sánchez-Baeza, F.; Granier, B.; Voirin, G.; Marco, M.-P. *Trends Anal. Chem.* **2009**, *28*, 769–777. (b) Adrian, J.; Pasche, S.; Pinacho, D. G.; Diserens, J.-M.; Sánchez-Baeza, F.; Gao, H.; Marco, M.-P.; Voirin, G. *Biosens. Bioelectron.* **2009**, *24*, 3340–3346.
- (6) Suárez, G.; Jin, Y.-H.; Auerswald, J.; Berchtold, S.; Knapp, H. F.; Diserens, J.-M.; Leterrier, Y.; Manson, J.-A. E.; Voirin, G. *Lab Chip* **2009**, *9*, 1625–1630.
- (7) (a) Knoll, W. *Annu. Rev. Phys. Chem.* **1998**, *49*, 569–638. (b) Bada, A.; Advincula, R. C.; Knoll, W. In *Novel Methods To Study Interfacial Layers*; Möbius, D., Miller, R., Eds.; Studies in Interface Science, Vol. 11; Elsevier Science: New York, 2001; p 55.
- (8) (a) Homola, J. *Surface Plasmon Resonance Based Sensor*; Springer: Berlin, Germany, 2006. (b) Hoa, X. D.; Kirk, A. G.; Tabrizian, M. *Biosens. Bioelectron.* **2007**, *23*, 151–160. (c) Homola, J. *Chem. Rev.* **2008**, *108*, 462–493.
- (9) (a) Fivash, M.; Towler, E. M.; Ficher, R. J. *Curr. Opin. Biotechnol.* **1998**, *9*, 97–101. (b) Cooper, M. A. *Nat. Rev. Drug Discovery* **2002**, *1*, 515–528. (c) Shankaran, D. R.; Gobi, K. V. A.; Miura, N. *Sens. Actuators, B* **2007**, *121*, 158–177.

Scheme 1. Molecular Structures and MRL Levels of Antibiotics Used in This Study



the analytes or small refractive index changes induced by low-molecular-weight analytes. For example, the conjugation of latex particles,¹² liposomes,¹³ or secondary proteins¹⁴ was used to amplify small refractive index changes and to generate observable SPR shifts. Metal nanoparticles, NPs (e.g., Au NPs or Ag NPs), exhibiting a localized plasmon, were extensively used to amplify SPR signals. The coupling of the localized plasmon of the NPs with the surface plasmon wave was found to affect the plasmon energy and, thus, to enhance the SPR shifts.¹⁵ Indeed, numerous studies have used Au NPs as amplifying labels for recognition events, and the effects of the size and the coverage of the Au NPs on the SPR responses were discussed.¹⁶ For example, the formation of immunocomplexes,¹⁷ DNA hybridization,¹⁸ and

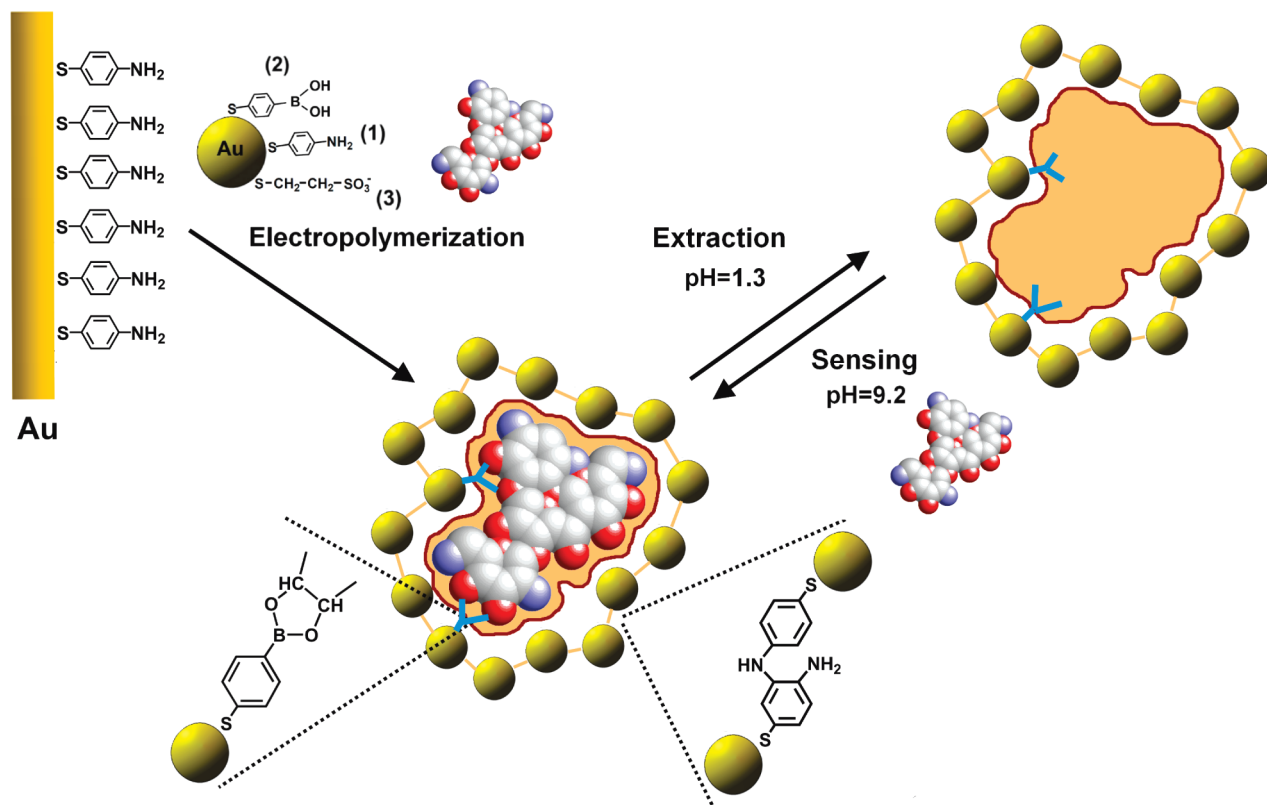
biocatalytic processes¹⁹ were followed by the amplification of the SPR signals using the Au NPs.

Recently, we reported on the development of an ultrasensitive trinitrotoluene (TNT) SPR sensor based on the electropolymerization of thioaniline-modified Au NPs on a thioaniline-functionalized Au surface that yields a bisaniline-cross-linked Au NP composite on the electrode surface.²⁰ It was demonstrated that upon the electropolymerization of the Au NPs in the presence of picric acid, acting as an imprint analogue of TNT, molecularly imprinted sites for the binding of TNT to the Au NP composite were generated. The imprinted sites revealed high affinities for the association of TNT, driven by π -donor–acceptor interactions between the bisaniline bridging units, and TNT and assisted by complementary steric constraints of the imprinted contours. This led to the selective association and high binding constants of TNT to the imprinted sites. The refractive index changes, and the accompanying SPR shifts, resulting from the formation of the π -donor–acceptor complexes between TNT and the bisaniline units in the imprinted sites, were, then, amplified by the coupling

(10) (a) Iwasaki, Y.; Horiuchi, T.; Niwa, O. *Anal. Chem.* **2001**, *73*, 1595–1598. (b) Raitman, O. A.; Katz, E.; Bückmann, A. F.; Willner, I. *J. Am. Chem. Soc.* **2002**, *124*, 6487–6496. (c) Tian, S.; Bada, A.; Liu, J.; Wang, Z.; Knoll, W.; Park, M.-K.; Advincula, R. *Adv. Funct. Mater.* **2003**, *13*, 473–484. (11) (a) Raitman, O. A.; Katz, E.; Willner, I.; Chegel, V. I.; Popova, G. V. *Angew. Chem., Int. Ed.* **2001**, *40*, 3649–3652. (b) Yao, X.; Wang, J.; Zhou, F.; Wang, J.; Tao, N. *J. Phys. Chem. B* **2004**, *108*, 7206–7212. (c) Zhai, P.; Guo, J.; Xiang, J.; Zhou, F. *J. Phys. Chem. C* **2007**, *111*, 981–986. (d) Sriwichai, S.; Bada, A.; Deng, S.; Huang, C.; Phanichphant, S.; Advincula, R. C. *Langmuir* **2008**, *24*, 9017–9023. (12) (a) Kubitschko, S.; Spinke, J.; Bruckner, T.; Pohl, S.; Oranthe, N. *Anal. Biochem.* **1997**, *253*, 112–122. (b) Besselink, G. A. J.; Kooyman, R. P. H.; van Os, P. J. H. J.; Engbers, G. H. M.; Schasfoort, R. B. M. *Anal. Biochem.* **2004**, *333*, 165–173. (13) Wink, T.; van Zuielen, S. J.; Bult, A.; van Bennekom, W. P. *Anal. Chem.* **1998**, *70*, 4763–4773. (14) Zayats, M.; Raitman, O. A.; Chegel, V. I.; Kharitonov, A. B.; Willner, I. *Anal. Chem.* **2002**, *74*, 4763–4773. (15) (a) Holland, W. R.; Hall, D. G. *Phys. Rev. B* **1983**, *27*, 7765–7768. (b) Lyon, L. A.; Musick, M. D.; Smith, P. C.; Reiss, B. D.; Peña, D. J.; Natan, M. J. *Sens. Actuators, B* **1999**, *54*, 118–124.

(16) (a) Schultz, D. A. *Curr. Opin. Biotechnol.* **2003**, *14*, 13–22. (b) Jain, P. K.; Huang, X.; El-Sayed, I. H.; El-Sayed, M. A. *Acc. Chem. Res.* **2008**, *41*, 1578–1586. (c) Anker, J. N.; Hall, W. P.; Lyandres, O.; Shah, N. C.; Zhao, J.; Van Duyne, R. P. *Nat. Mater.* **2008**, *7*, 442–453. (17) (a) Lyon, L. A.; Musick, M. D.; Natan, M. J. *Anal. Chem.* **1998**, *70*, 5177–5183. (b) Englebienne, P.; Hoonacker, A. V.; Verhas, M. *Analyst* **2001**, *126*, 1645–1651. (c) Mauriz, E.; Calle, A.; Lechuga, L. M.; Quintana, J.; Montoya, A.; Manclus, J. *Anal. Chim. Acta* **2006**, *561*, 40–47. (18) He, L.; Musick, M. D.; Nicewarner, S. R.; Salinas, F. G.; Benkovic, S. J.; Natan, M. J.; Keating, C. D. *J. Am. Chem. Soc.* **2000**, *122*, 9071–9077. (19) (a) Zayats, M.; Pogorelova, S. P.; Kharitonov, A. B.; Lioubashevski, E. K.; Willner, I. *Chem.—Eur. J.* **2003**, *9*, 6108–6114. (20) Riskin, M.; Tel-Vered, R.; Lioubashevski, O.; Willner, I. *J. Am. Chem. Soc.* **2009**, *131*, 7368–7378.

Scheme 2. Imprinting of Molecular Recognition Sites for Antibiotic Substrates (for Example, Neomycin) through the Electropolymerization of a Bisaniline-Cross-Linked Au NP Composite on a Au Surface



between the localized plasmon of the Au NPs and the surface plasmon wave. This enabled the ultrasensitive (1×10^{-14} M) detection of TNT.

In the present study we report on the synthesis of Au NPs modified with a composite capping monolayer consisting of the electropolymerizable thioaniline units and phenylboronic acid ligands that provide ligation sites for the association of different antibiotic substrates. The electropolymerization of the functionalized Au NPs in the presence of the antibiotic substrates yields imprinted NP composites that carry ligands which enable the selective SPR sensing of different antibiotics. The sensing matrixes are used to analyze the antibiotics in milk.

Boronic acids and vicinal diols form cyclic boronate complexes, which can be reversibly dissociated and reassociated under acidic or basic conditions, respectively. These functions of the boronic acid ligand were used to synthesize molecularly imprinted polymers for vicinal diol-functionalized substrates, such as saccharides,²¹ and such imprinted polymers were used as specific recognition elements of sensor devices.²²

In the present study we used 3.5 nm Au NPs protected with a capping layer consisting of three components: thioaniline (1), acting as electropolymerizable units, (mercaptophenyl)boronic acid (2), acting as a ligand for the association of the antibiotic substrates, and mercaptoethanesulfonic acid (3), which stabilizes the NPs and prevents their precipitation. A Au-coated glass

electrode was modified with a thioaniline monolayer and used for the electrochemical deposition of the functionalized Au NPs, Scheme 2. The electropolymerization was conducted in the absence of the antibiotic substrate, to yield the nonimprinted bisaniline-cross-linked Au NP composite or in the presence of one of the antibiotic substrates neomycin (NE, 4), kanamycin (KA, 5), or streptomycin (ST, 6), to yield the imprinted bisaniline-cross-linked Au NP composites. Following the imprinting process, the imprinted substrate was eliminated from the matrix under acidic conditions (pH 1.3), and the electrode was, then, equilibrated with a basic buffer solution (pH 9.2). The electropolymerization of the Au NP matrixes included the application of 10 voltammetric cycles between -0.35 and $+0.85$ V vs a Ag quasi-reference electrode, followed by an application of a fixed potential of 0.85 V for 60 min, and was probed in situ by the surface plasmon resonance shifts of the surface (see Figure S1, Supporting Information). The surface was characterized by AFM (Figure S2, Supporting Information), and it exhibited an average thickness of ca. 11 nm and included aggregated Au NP structures with heights up to 35 nm. The microgravimetric quartz-crystal-microbalance analysis of the electrodeposited Au NPs on a Au-quartz crystal revealed a mass change of $8.7 \times 10^{-6} \text{ g} \cdot \text{cm}^{-2}$ that translated to an average coverage of ca. three random densely packed layers of the Au NPs.

Figure 1A depicts the SPR curve of the NE-imprinted Au NP composite before, curve a, and after, curve b, treatment of the matrix with 200 nM NE. A clear shift of the SPR spectrum is observed upon the binding of NE to the Au NP matrix. Figure 1B shows the derived sensogram, measured at $\theta = 63.5^\circ$, that corresponds to the reflectance changes of the NE-imprinted Au NP composite surface upon interaction with increasing concentra-

- (21) (a) Wulff, G.; Gimpel, J. *Makromol. Chem.* **1982**, *183*, 2469–2477. (b) Wulff, G.; Schauhoff, S. *J. Org. Chem.* **1991**, *56*, 395–400. (c) Wulff, G.; Schmidt, H.; Witt, H.; Zentel, R. *Angew. Chem., Int. Ed. Engl.* **1994**, *33*, 188–191.
 (22) (a) Sallacan, N.; Zayats, M.; Bourenko, T.; Kharitonov, A. B.; Willner, I. *Anal. Chem.* **2002**, *74*, 702–712. (b) Pogorelova, S. P.; Zayats, M.; Bourenko, T.; Kharitonov, A. B.; Lioubashevski, O.; Katz, E.; Willner, I. *Anal. Chem.* **2003**, *75*, 509–517.

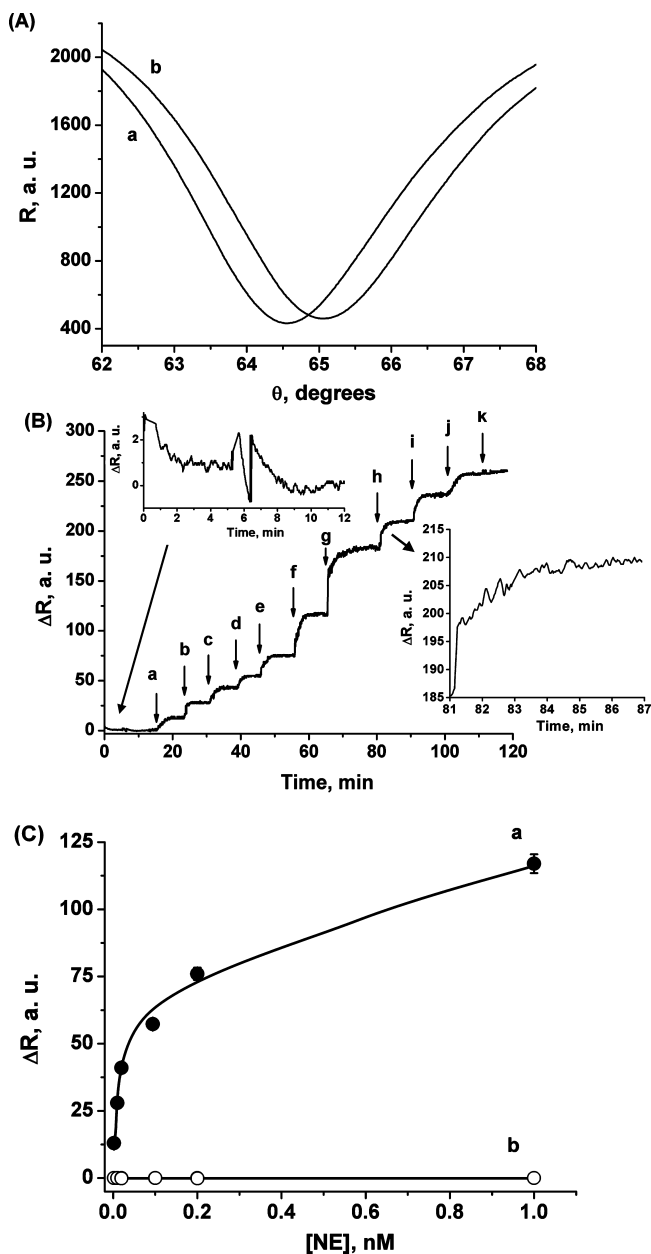


Figure 1. (A) SPR curves corresponding to the NE-imprinted bisaniline-cross-linked Au NP composite: (a) before the addition of NE and (b) after the addition of NE, 200 nM. (B) Sensogram corresponding to the changes in the reflectance intensities, at $\theta = 63.5^\circ$, by the NE-imprinted bisaniline-cross-linked Au NP composite upon addition of variable concentrations of NE: (a) 2 pM, (b) 10 pM, (c) 20 pM, (d) 100 pM, (e) 200 pM, (f) 1 nM, (g) 4 nM, (h) 20 nM, (i) 100 nM, (j) 200 nM, (k) 1 μ M. Arrows indicate the time of addition of the analyte. Left inset: Enlarged time-dependent reflectance values measured for the bulk HEPES buffer. Right inset: Enlarged time-dependent reflectance changes upon the addition of 20 nM NE. (C) Calibration curves corresponding to the reflectance changes at different concentrations of added NE on (a) the NE-imprinted bisaniline-cross-linked Au NP composite and (b) the nonimprinted bisaniline-cross-linked Au NP composite. Error bars correspond to a set of $N = 5$ measurements. All measurements were performed in a 0.1 M HEPES buffer solution (pH 9.2).

tions of NE. Figure 1B, right inset, shows a magnified region of the time-dependent reflectance change upon interaction of the matrix with NE. One may realize that after ca. 5 min the reflectance changes level off to a constant value, meaning that

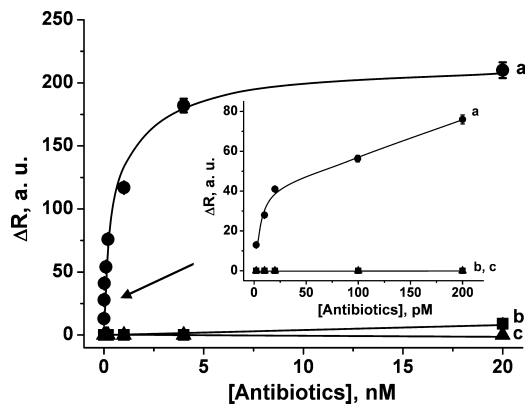


Figure 2. Calibration curves corresponding to the analysis of various concentrations of (a) NE, (b) KA, and (c) ST on an NE-imprinted bisaniline-cross-linked Au NP composite. Inset: Lower concentration region of the calibration curves. Error bars correspond to a set of $N = 5$ measurements. All measurements were performed in a 0.1 M HEPES buffer solution (pH 9.2).

the response time of the sensing matrix is ca. 5 min. The resulting calibration curve for sensing NE by the NE-imprinted Au NP composite is shown in Figure 1C, curve a. For comparison, the reflectance changes upon the interaction of the nonimprinted Au NP composite with NE are shown in Figure 1C, curve b. The reflectance changes observed with the imprinted matrix are significantly higher, implying the improved binding of NE to the imprinted matrix. This is explained by the fact that the electropolymerization of the Au NPs, in the presence of NE molecules, yields molecularly imprinted sites with structural contours for NE. The sites include the boronic acid ligands in optimal positions inside the imprinted domains for binding NE (Scheme 2). The detection limit for analyzing NE by the imprinted matrix corresponds to 2.00 ± 0.21 pM (for the determination of the detection limit see the Experimental Section).

A further aspect relates to the effect of the Au NPs on the amplified detection of NE by the sensing composite. Toward this end, we modified the Au surface with a (mercaptophenyl)boronic acid monolayer that lacked the Au NPs. The association of NE to the monolayer-modified electrode was, then, followed by probing the reflectance changes at different concentrations of NE (Figure S3, Supporting Information). One may realize that the ligand-functionalized monolayer surface detects NE at a 1 μ M concentration, implying a ca. 10^3 amplification factor of the nonimprinted Au NP composite and a further 10^3 amplification factor of the imprinted sensing interface.

An important aspect in the sensing of NE by the NE-imprinted Au NP matrix relates to the specificity of the analysis in the presence of other vicinal diol-functionalized antibiotics. Figure 2 shows the reflectance changes observed upon the interaction of the NE-imprinted Au NPs with NE, curve a, and upon the interaction of the sensing matrix with the “foreign” antibiotic KA, curve b, or ST, curve c. Clearly, an impressive selectivity is demonstrated by the NE-imprinted Au NP composite. While the imprinted matrix reveals measurable reflectance changes in the concentration range of 2 pM to 20 nM, the antibiotics KA and ST show almost no reflectance changes in this concentration range.

Similarly, KA and ST bearing vicinal hydroxyl groups were ligated to the phenylboronic acid-functionalized Au NPs and

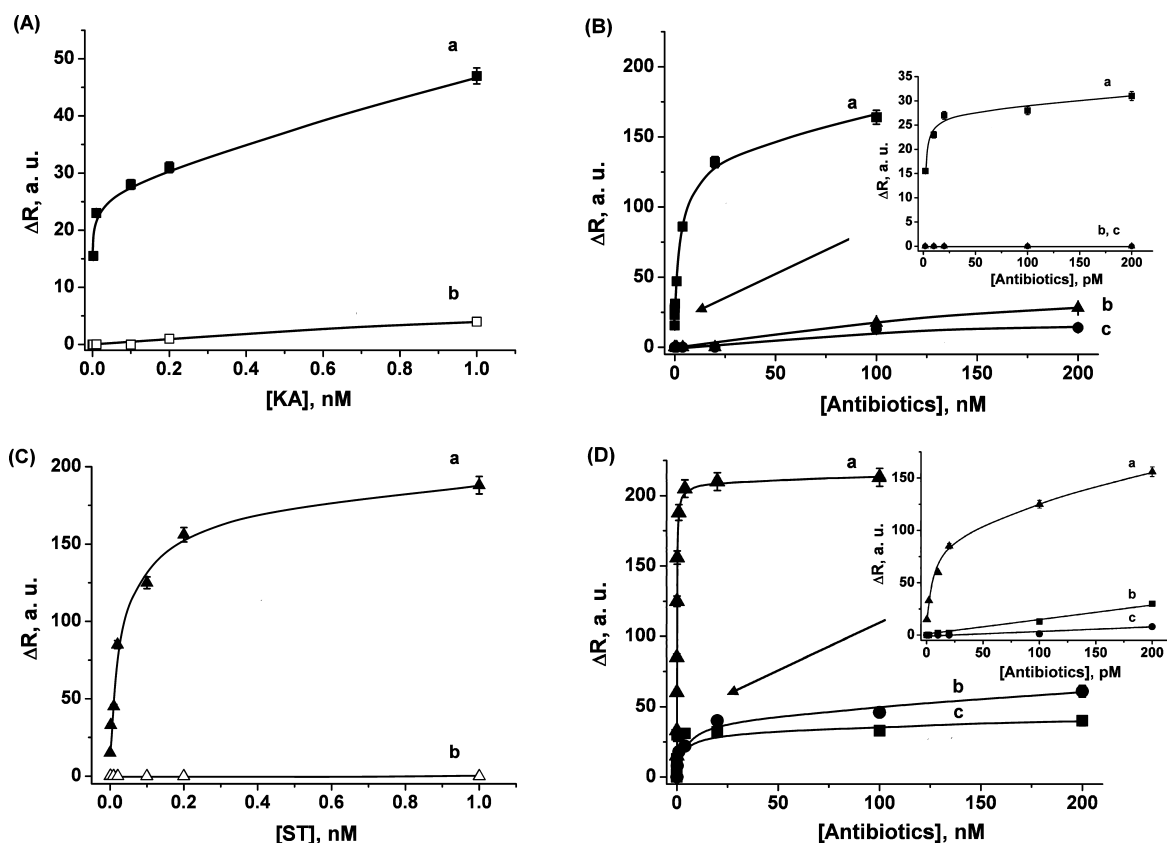


Figure 3. (A) Calibration curves corresponding to the reflectance changes at different concentrations of added KA on (a) the KA-imprinted bisaniline-cross-linked Au NP composite and (b) the nonimprinted bisaniline-cross-linked Au NP composite. (B) Calibration curves corresponding to the analysis of various concentrations of (a) KA, (b) ST, and (c) NE on a KA-imprinted bisaniline-cross-linked Au NP composite. Inset: Lower concentration region of the calibration curves. (C) Calibration curves corresponding to the reflectance changes in the presence of different concentrations of added ST to (a) the ST-imprinted bisaniline-cross-linked Au NP composite and (b) the nonimprinted bisaniline-cross-linked Au NP composite. (D) Calibration curves corresponding to the analysis of various concentrations of (a) ST, (b) NE, and (c) KA using the ST-imprinted bisaniline-cross-linked Au NP composite. Inset: Low concentration region of the calibration curves. Error bars correspond to a set of $N = 5$ measurements. All measurements were performed in a 0.1 M HEPES buffer solution (pH 9.2).

imprinted into the electropolymerized bisaniline-bridged Au NP matrixes assembled on the Au surfaces. The release of KA or ST from the Au NP composites, under acidic conditions, resulted in the imprinted sensing surfaces. Figure 3A, curve a, shows the calibration curve corresponding to the reflectance changes, ΔR , upon reaction of the KA-imprinted Au NP matrix with different concentrations of KA. As the concentration of KA increases, the observed reflectance changes are intensified. For comparison, Figure 3A, curve b, shows the reflectance changes of the nonimprinted Au NP composite upon the interaction with variable concentrations of KA. Clearly, the reflectance changes are substantially lower, suggesting the lower binding affinity of KA to the nonimprinted matrix. The detection limit for analyzing KA by the imprinted Au NP composite corresponded to 1.00 ± 0.10 pM, whereas the detection limit for sensing KA by the nonimprinted sensing interface was 1.00 ± 0.12 nM. The higher reflectance changes and the lower detection limit by the imprinted Au NP composite are attributed to the formation of the molecularly imprinted sites in the Au NP matrix that provide molecular structural contours and phenylboronic acid ligands for the steric accommodation of the KA substrate. Thus, the steric fit of KA to the imprinted sites increases the binding affinity of KA to the sensing matrix, and this leads to the lower detection limit. The

selectivity of the sensing matrix was also examined, Figure 3B. The differences in the reflectance changes of the KA-imprinted matrix in the presence of added KA, curve a, and upon interaction with ST, curve b, and NE, curve c, demonstrate an impressive selectivity. While KA is effectively detected in the concentration range of 1 pM to 1 nM, the interaction of the matrix with ST or NE does not show any significant reflectance changes at these concentrations.

The ST-imprinted Au NP composite reveals similar improved sensing properties. The ST-imprinted Au NP composite reveals a detection limit of 200 ± 30 fM, Figure 3C, curve a, while the nonimprinted Au NP matrix shows significantly lower reflectance values at these concentrations, Figure 3C, curve b. As before, the ST-imprinted Au NP composite reveals selectivity, Figure 3D, and while high reflectance changes are observed for analyzing the imprinted substrate ST, Figure 3D, curve a, only minute reflectance changes are observed upon interaction of the ST-imprinted matrix with NE, curve b, or KA, curve c.

To highlight the significance of the formation of the boronate complexes between the phenylboronic acid ligand and the vicinal hydroxyl groups of the NE, KA, or ST antibiotic in the formation of the imprinted sensing matrixes, we tried to imprint the enrofloxacin substrate (EN, **7**) into the bisaniline-cross-linked Au

NP layer. EN does not include vicinal hydroxyl groups (e.g., Scheme 1), and hence, this antibiotic cannot form the active boronate complex for imprinting. Accordingly, EN was interacted with the phenylboronic acid-functionalized Au NPs, and these were electropolymerized on the thioaniline-modified Au surface. The rinsed Au NP composite was, then, interacted with EN. Under these conditions, we did not observe any reflectance change up to an EN concentration of 1 μM . At this high concentration of the analyte, a minute reflectance change was observed, presumably due to a change in the refractive index of the solution. Thus, we conclude that the vicinal hydroxyl groups in NE, KA, and ST are essential to form the imprinted sites through the formation of the boronate complexes on the electropolymerizable Au NPs.

We, then, attempted to analyze the three antibiotic components in milk samples taken from three different local milk producers (milk samples 1–3, fat content in all samples 3%). The interaction of the milk sample with the imprinted Au NP composite resulted in a substantial reflectance change that, presumably, originated from the change of the refractive index of the buffer solution and/or was due to a nonspecific adsorption to the matrix. The high sensitivity of the imprinted Au NP matrixes and the MRL values defined by the health authorities suggest, however, that the milk samples can be substantially diluted, while still allowing the quantitative analysis of the antibiotics in the milk samples. Accordingly, the milk samples were 5000-fold diluted. The interaction of the NE-imprinted Au NP composite with the diluted milk samples did not induce any substantial reflectance changes; cf. Figure 4A, point a. Treatment of the NE-imprinted Au NP composite with 5000-fold-diluted milk samples that included different concentrations of NE yielded the reflectance changes depicted in the sensogram presented in Figure 4A. From the respective calibration curve, shown in Figure 4B, we realize that a NE concentration as low as 10 pM is detectable in the diluted milk sample. The MRL value for NE in milk is 1.65×10^{-6} M, a value that translates to a concentration that corresponds to 330 pM in a 5000-fold-diluted sample. Thus, our sensor system reveals the sensitivity to detect the MRL as well as lower levels of NE. Similarly, KA-imprinted and the ST-imprinted Au NP composites were used for analyzing KA and ST in the diluted milk samples, respectively, Figure 4B. The MRLs for KA and ST are 2.6×10^{-7} and 1.4×10^{-7} M, respectively. These values translate to concentrations of 52 and 28 pM, respectively, for the KA and ST in the 5000-fold-diluted milk samples. From the calibration curves shown in Figure 4B, we realize that the two antibiotics can be detected in the diluted samples significantly below the MRL values (the observable detection limits for KA and ST are 2.00 ± 0.10 pM and 200 ± 21 fM, respectively). Moreover, the absence of SPR responses during the introduction of the diluted milk samples suggests that the milk samples of all three local manufacturers were not contaminated by any of the three antibiotics NE, KA, and ST. This observation was further supported by performing complementary internal standard addition experiments, Figure S4, Supporting Information. In these experiments, variable concentrations of ST, KA, or NE were added to any one of the milk samples, and the recorded reflectance changes provided a quantitative measure for the content of the added antibiotic. Figure S4, inset, exemplifies the resulting calibration curve obtained for analyzing NE on the NE-

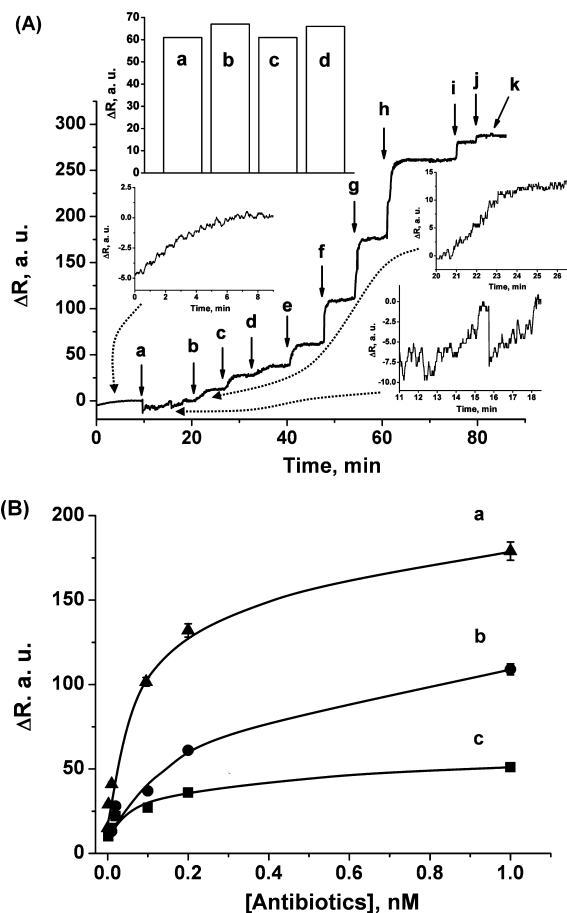


Figure 4. (A) Sensogram corresponding to the changes in the reflectance intensities, at $\theta = 63.5^\circ$, at the NE-imprinted bisaniline-cross-linked Au NP composite upon analysis of a milk sample. The measurement begins with a pure 0.1 M HEPES buffer solution (pH 9.2) in the absence of NE. Point a corresponds to the addition of milk sample 1 diluted 5000-fold with the HEPES buffer solution. The following NE concentrations were subsequently added to the 5000-fold-diluted milk sample: (b) 10 pM, (c) 20 pM, (d) 100 pM, (e) 200 pM, (f) 1 nM, (g) 4 nM, (h) 20 nM, (i) 100 nM, (j) 200 nM, (k) 1 μM . Arrows indicate the time of addition of the analyte. Also presented are three insets, depicting magnified regions corresponding to reflectance intensity changes by (lower left) the bulk HEPES buffer, (lower right) milk sample 1 diluted 5000-fold in the HEPES buffer solution, and (upper right) milk sample 1 diluted 5000-fold with the HEPES buffer solution with added NE, 10 pM. Upper left inset: Reflectance changes, by the NE-imprinted Au NP composite-modified Au electrode, corresponding to the analysis of milk sample 1 diluted 5000-fold with 0.1 M HEPES buffer solution (pH 9.2) and containing (a) 200 pM NE, (b) 200 pM NE, 10 pM KA, and 100 pM ST, (c) 200 pM NE, 50 pM KA, and 50 pM ST, and (d) 200 pM NE, 100 pM KA, and 10 pM ST. (B) Calibration curves corresponding to the analysis of various concentrations of (a) ST, (b) NE, and (c) KA on the bisaniline-cross-linked Au NP composites imprinted with the respective antibiotics. Measurements were performed in milk sample 1 diluted 5000-fold with a 0.1 M HEPES buffer solution (pH 9.2).

imprinted matrix in one of the milk samples. By extrapolation of the plot to $\Delta R = 0$, the content of the antibiotic was estimated. In this specific example, the concentration of NE was estimated to be ≤ 8 pM, far below the MRL values. Similar results were obtained for the other antibiotics (Figure S5, Supporting Information), leading to the conclusion that the residual content of antibiotics in all three samples was below the MRL values. Also,

it should be noted that the NE–Au NP for composite could be regenerated at least five times, and the results analyzing variable concentrations of NE revealed an impressive reproducibility of $\pm 3\%$.

We also find that the imprinted Au NP composites allow the selective analysis of antibiotics added to the milk samples. For example, Figure 4, upper left inset, shows the reflectance changes of the NE-imprinted composite upon analysis of NE, 200 pM (column a), and upon the addition of different concentrations of KA or ST, columns b–d, to the NE solution. Clearly, the foreign nonimprinted antibiotics do not have any significant effect on the reflectance changes. Similar results were observed for analyzing KA or ST by the respectively imprinted Au NP composites upon the addition of the nonimprinted antibiotics to the solution containing the imprinted antibiotic (see Figure S6, Supporting Information). The method to fabricate the imprinted cross-linked Au NP composites by electrochemical means represents a major advantage in the future design of SPR chips for the parallel sensing of the different antibiotics. By using an electrode array, the different sensing matrixes may be addressed to specific electrodes, thus enabling the parallel analysis of the substrates.

To conclude, we have demonstrated the use of electropolymerizable thioaniline-modified Au NPs capped with phenylboronic acid ligand as a functional material for the development of sensitive and selective matrixes for the detection of a series of antibiotics that include vicinal hydroxyl groups in their molecular structure. The electropolymerization of the NPs on a Au surface in the presence of NE, KA, or ST led to the formation of molecularly imprinted Au NP matrixes. The imprinted composites revealed high sensitivity and specificity toward the detection of the imprinted antibiotic substrates. The binding processes of the antibiotic analytes to the imprinted sites were probed by surface plasmon resonance spectroscopy. The detection of the antibiotics by the matrixes was amplified due to the changes in the dielectric properties of the matrixes, occurring upon the binding of the substrates to the imprinted sites, through the coupling of the localized plasmon of the NPs with the surface plasmon wave. The different sensing matrixes were successfully applied to analyze the antibiotic substrates in milk samples. The selectivity demonstrated by the different imprinted Au NP composites toward the sensing of the imprinted antibiotic substrates, suggests that electropolymerized imprinted Au NP composites addressed on Au arrays could be implemented for the parallel SPR analysis of the antibiotic substrates.

EXPERIMENTAL SECTION

Synthesis of the Functionalized Au Nanoparticles. Au nanoparticles functionalized with 2-mercaptoethanesulfonic acid, *p*-aminothiophenol, and (*p*-mercaptophenyl)boronic acid (Au NPs) were prepared by mixing a 10 mL solution containing 197 mg of HAuCl₄ in ethanol and a 5 mL solution containing 36 mg of 2-mercaptoethanesulfonic acid, 10 mg of (*p*-mercaptophenyl)-boronic acid, and 8 mg of *p*-aminothiophenol in methanol. The two solutions were stirred in the presence of 2.5 mL of glacial acetic acid in an ice bath for 1 h. Subsequently, a 7.5 mL aqueous solution of 1 M sodium borohydride, NaBH₄, was added dropwise, resulting in a dark color solution associated with the presence of the Au NPs. The solution was stirred for an additional 1 h in an ice bath and, then, for 14 h at room

temperature. The particles were successively washed and centrifuged (twice in each solvent) with methanol, ethanol, and diethyl ether. A mean particle size of ca. 3.5 nm was determined using TEM.

Preparation of the Au-NP-Modified Au Surfaces. *p*-Aminothiophenol-functionalized electrodes were prepared by immersing Au-coated glass slides for 24 h in a *p*-aminothiophenol ethanolic solution, 10 mM. To prepare the bisaniline-cross-linked Au NP composite, a 2 mg·mL⁻¹ of the functionalized Au NPs were dissolved in a 0.1 M HEPES buffer solution (pH 9.2), and were electropolymerized on the *p*-aminothiophenol-modified Au electrode. Electropolymerization was performed by the application of 10 potential cycles between -0.35 and $+0.85$ V vs a Ag wire quasi-reference electrode (QRE), at a scan rate of 100 mV·s⁻¹, followed by the application of a constant potential, $E = 0.85$ V vs a Ag QRE, for 60 min. The resulting films were, then, washed with the background buffer solution to exclude any residual monomer from the electrode. Similarly, antibiotic-imprinted bisaniline-cross-linked films were prepared by reacting 2 mg of the modified Au NPs, prior to the electropolymerization process, with 2 mL of HEPES buffer solution (pH 9.2) that included 10 mM of the selected antibiotic, and allowing the antibiotic–Au NP complex to precipitate for 30 min. The precipitate was separated, washed, and redissolved in 4 mL of 0.1 M HEPES buffer (pH 9.2) to yield the electropolymerization solution for the imprinted matrixes.

The extraction of the antibiotic molecules from the film was carried out by immersing the electrodes in a 0.1 M H₂SO₄ (pH 1.3) solution for 15 min and thoroughly washing with a HEPES buffer solution (pH 9.2). The full removal of the antibiotic molecules from the electropolymerized film was verified by monitoring the SPR curve until a steady curve shape was obtained.

Instrumentation. An SPR Kretschmann-type spectrometer, NanoSPR 321 (NanoSPR devices), with a LED light source, $\lambda = 650$ nm, and a prism refraction index $n = 1.61$ was used. The SPR measurements were performed using a home-built cell, volume 0.5 mL. Electropolymerization was performed using a Pt wire (diameter 0.5 mm) counter electrode and a Ag wire quasi-reference electrode (diameter 0.5 mm) which were installed in the SPR cell (volume 0.5 mL, working electrode area 0.2 cm²). Au-coated semitransparent glass plates (Mivitec GmbH, Analytical μ -Systems, Germany) were used as working electrodes. Prior to modification, the Au surface was cleaned in hot ethanol (50 °C) for 20 min.

For the electropolymerization process a PC-controlled (Autolab GPES software) electrochemical analyzer potentiostat/galvanostat (μ Autolab, type III) was employed. AFM imaging was performed at room temperature using a multimode scanning probe microscope with a Nanoscope 3A controller (Digital Instruments, Veeco Probes). The image was taken with an NSC 15 AFM tip (Mikromasch, Germany) using the tapping mode at its resonant frequency. The image was analyzed with WsXM SPIP software (Nanotec, Inc., Spain). QCM measurements were performed using a home-built instrument linked to a frequency analyzer (Fluke) using Au-quartz crystals (AT-cut 10 MHz). Nanopure (Barnstead) ultrapure water was used in the preparation of the different solutions.

Analysis of the Antibiotic Substances. The NE-, KA-, or ST-imprinted Au NP matrixes were subjected to different concentrations of the respective antibiotic substances. Sensograms were recorded at a fixed reflection angle corresponding to 63.5° . The detection limit confidence intervals were estimated according to the IUPAC recommendations where the detection limit (C_L) is “the lowest detectable concentration that can be detected with reasonable certainty”, and is given by $C_L = \bar{C}_n + tS_n/\sqrt{n}$, where \bar{C}_n is the average value of the lowest detectable concentration, t is the Student factor chosen according to a 95% confidence level and using $n = 5$ measurements, and S_n is the measured standard deviation for five separate measurements.

ACKNOWLEDGMENT

This research is supported by the Converging Technologies Program, The Israel Science Foundation. M.R. is supported by the CAMBR fellowship.

SUPPORTING INFORMATION AVAILABLE

Additional information as noted in text. This material is available free of charge via the Internet at Web at <http://pubs.acs.org>.

Received for review December 23, 2009. Accepted February 4, 2010.

AC902944K